## Detection of Hidden Faults in Electric Power Facilities Combining SAM and U-Net

Ran Duan, Chunguang Ma\*

AIEN Institute, Shanghai Ocean University, Shanghai China, 2391413@st.shou.edu.cn, cgma@shou.edu.cn

Keywords: Electric Power Facilities, Hidden Fault, Infrared Imaging, SAM, U-Net.

#### Abstract

Fault detection in electric power facilities is a crucial component of power grid maintenance, with hidden faults posing greater challenges compared to overt faults. Notably, hidden faults often coincide with localized heating, making infrared imaging an effective detection modality. However, automatic identification of power equipment in infrared images remains challenging; traditional methods are often inefficient and lack accuracy, while deep learning approaches are hindered by limited sample availability and accuracy issues. Furthermore, the temperature-based criteria for diagnosing hidden faults lack robustness. To address these challenges, this study proposes a comprehensive approach: first, employing the Segment Anything Model (SAM) for rapid annotation of power facilities in infrared images; second, leveraging these annotations to iteratively optimize a U-Net model for automated power equipment identification; and third, integrating temperature information to identify abnormal regions using dynamic threshold segmentation, thereby locating potential fault components. Experimental validation was conducted on a transmission line in Jiaxing City, Zhejiang Province, demonstrating a detection success rate exceeding 90%. The results indicate high detection accuracy and efficiency, presenting a promising solution for intelligent inspection of electric power infrastructure.

#### 1. Introduction

With the ongoing advancement of society and technology, the global demand for electrical power resources continues to rise. In the context of large-scale electrical infrastructure construction, efficiently identifying and mitigating potential safety hazards within complex environments, as well as ensuring the safe and stable operation of electrical facilities, has become a critical yet challenging issue in modern electrical facility management (Impram, S. et al., 2020; Strielkowski, W. et al., 2021). Traditionally, fault detection in electrical facilities such as transmission lines relied heavily on manual inspections and visual observation, where faults were identified through human visual assessment. However, this approach suffers from low efficiency, limited fault tolerance, and high human resource consumption, rendering it inadequate to meet the increasing demand for electrical resources and the high dependence on electrical infrastructure (Dashti, R. et al., 2021).

To enhance fault detection and operational maintenance efficiency, the application of unmanned aerial vehicles (UAVs) for photographic inspection of electrical facilities has garnered significant attention (Abro, G. et al., 2024; Barbedo, J. G. A., 2019). The prevalent UAV-based power inspection methodology involves equipping UAVs with visible light cameras to capture images of electrical infrastructure, followed by image recognition techniques to analyze these images for fault detection. Such methods are relatively mature and have been widely adopted in various electrical institutions, effectively identifying surface-level faults such as issues in incoming and outgoing cable heads, insulation flashovers, fuse drop-outs, and line trips caused by vegetation interference (Susakova, T. et al., 2017).

However, these visible light-based approaches face significant limitations—they are incapable of detecting covert faults within electrical components, such as faults in voltage transformers, current transformers, relay protection terminals, or coil heating resulting from prolonged energization (Liao, W. et al., 2021; Mateus, B. et al., 2024). These covert faults are often critical precursors to more severe failures, including transmission line short circuits, power outages, fires, and conductor breaks, necessitating further investigation. Since covert faults typically manifest as localized heating without visible surface changes, they are indistinguishable from normal components in standard visible light images. Conversely, infrared imaging captures thermal infrared radiation and is highly sensitive to temperature variations in targets (McManus, C. et al., 2016; Hou, F. et al.,

2022). Consequently, infrared thermography provides a valuable means for detecting and analyzing temperature anomalies in electrical equipment, enabling the identification of thermally compromised components and facilitating early fault detection.

Infrared imaging offers a promising approach for the detection of covert faults in electrical facilities. However, practical implementation faces several challenges, primarily the accurate identification of electrical components within infrared images. Traditional manual inspection methods are inefficient, laborintensive, and prone to inaccuracies, which hinder timely fault detection (Cheng, F. et al., 2023; Hedayati, M. et al., 2024; Sarabandi, K. et al., 2002). Consequently, numerous studies have explored automatic identification techniques for electrical facilities. For instance, Mira J. employed a HOG+SVM scheme for efficient and accurate detection of olive fly larvae on edge devices, detailing feature extraction and classification workflows (Mira J., 2024). Wang G. applied Haar+AdaBoost to detect longitudinal tears in conveyor belts under uneven illumination, achieving a 3% error rate (Wang G., 2021). Zhang et al. utilized Hough transform-based methods for power line segmentation, combined with K-means clustering and Kalman filtering for line tracking (Zhang, J. et al., 2012). Seikh et al. enhanced line detection success rates to 83% through fine edge map-based Hough transform techniques (Seikh, N. et al., 2022). Despite these advances, traditional methods often suffer from limited real-time performance, prolonged training durations, and suboptimal accuracy.

With the advent of deep learning, significant improvements have been achieved in automatic electrical facility recognition. For example, Ma et al. improved the YOLO-based framework for transmission line detection (Ma, W. et al., 2024), while Zheng et al. enhanced Faster R-CNN with deformable convolutions and transfer learning to detect power towers in remote sensing imagery, increasing detection metrics by 0.2 points (Zheng, X. et al., 2020). Zhao et al. proposed PL-UNet, specifically tailored for power line recognition, further improving detection capabilities (Zhao, Q. et al., 2025). Nan G. et al. employed AS-Unet++ to extract electrical facilities from remote sensing data with higher accuracy (Nan G. et al., 2024), and He et al. utilized an improved U-Net architecture for efficient feature extraction (He, M. et al., 2023). Compared to classical algorithms, deep learning approaches, especially U-Net variants, have demonstrated superior precision and robustness in target recognition, offering a feasible pathway toward fully automated electrical facility identification. However, most

existing studies focus on visible light images; research on infrared imagery remains limited. Since dataset quality critically impacts model performance (Zou, X. et al., 2019; Kaur, R. et al., 2023; Manakitsa, N. et al., 2024), establishing representative infrared datasets and targeted training paradigms are essential for robust recognition.

Constructing such datasets is labor-intensive, especially due to the complex geometries and overlapping structures typical of electrical facilities, as illustrated in Figure 1, the shape of the power facilities is very complex, and manual labeling takes a lot of time. To address this, this study proposes utilizing the Segment Anything Model (SAM) for rapid, accurate annotation of infrared images, facilitating subsequent training of a U-Net-based model for power facility recognition.

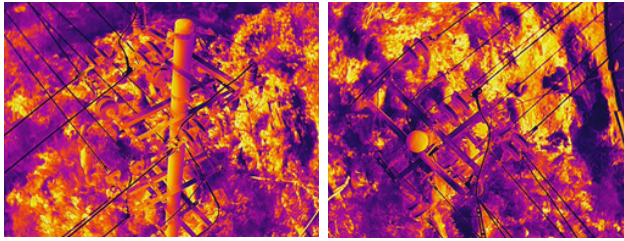


Figure. 1. Complex electric power facilities

A further challenge in infrared-based fault detection involves defining temperature thresholds for identifying hidden faults. The thermal behavior of electrical components is influenced by load current, aging, ambient temperature, and environmental factors (Islam, M. et al., 2024; Junior, O. et al., 2023). Normal temperature fluctuations often overlap with early fault signatures, complicating diagnosis—for example, a circuit breaker measuring 85°C during summer heatwaves may be normal or indicative of an early fault depending on contextual factors such as load and ambient temperature. The relationship between equipment aging and temperature is nonlinear; newly installed units may temporarily exhibit anomalous temperatures due to surface treatments, while aged components can display altered thermal profiles caused by material degradation (Zhu, M. et al., 2024). External environmental conditions, such as sunlight exposure, wind speed, and thermal radiation from adjacent equipment, further impact temperature measurements accuracy (Wan, Q. et al., 2021).

Typically, early-stage faults manifest as localized temperature anomalies—such as hotspots in cable joints or regional heating in insulators—requiring dynamic and adaptive thresholding strategies for effective detection. The key to accurate fault diagnosis lies in establishing a temperature threshold model that accounts for multi-dimensional factors, including historical data, environmental conditions, and operational parameters, to distinguish true faults from benign temperature variations.

In summary, this study employs the Segment Anything Model (SAM) to facilitate rapid annotation of power facilities in infrared imagery. Subsequently, an iterative optimization approach is applied to refine the U-Net model using the annotated data, enabling automated identification of power facilities. Finally, by integrating temperature information, the method utilizes threshold segmentation to detect abnormal regions in infrared images, thereby identifying components with hidden faults. The main contributions of this work are as follows:

- 1. Developing a SAM-assisted rapid annotation framework for power facilities in infrared images.
- 2. Proposing an iterative training strategy that combines SAM annotations with U-Net optimization to achieve automatic power facility recognition.

3. Establishing a dynamic temperature thresholding model for effective discrimination of hidden faults in infrared thermal images.

The structure of this study is as follows: Part 1 presents the problems addressed in this paper and the current state of the field. Part 2 provides a detailed description of the methodology we propose. Part 3 focuses on the experiments, detailing the performance of a real-world dataset processed using the approach outlined in this paper. Part 4 consists of the conclusions.

## 2. Methodology

This study proposes a method for fault detection in power facilities using infrared thermal imaging. First, an infrared image dataset of power facilities is generated utilizing the Segment Anything Model (SAM) to facilitate efficient annotation. This dataset is then employed to train a U-Net model for automatic recognition of power facilities. Subsequently, by integrating temperature data and applying threshold segmentation, abnormal regions within the infrared images are identified, enabling the detection of concealed faulty components. The overall workflow of the proposed approach is illustrated in Figure 2.

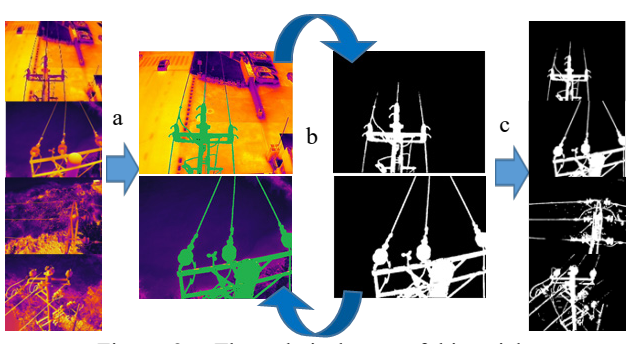


Figure. 2. The technical route of this article

The first step of the process involves using the SAM algorithm to segment the input thermal infrared image, illustrated in Figure 2(a). Subsequently, the segmentation results are manually confirmed and edited to produce accurate segmentation outcomes (This process will be repeated multiple times), illustrated in Figure 2(b). After that, the UNet model is trained using the thermal infrared images and the accurate segmentation results as samples. Finally, the trained model is applied to recognize any thermal infrared image, and the power facility recognition results are output, illustrated in Figure 2(c).

# 2.1 SAM assisted labeling of power facilities and optimization of U-Net

## **2.1.1** The SAM

The Segment Anything Model (SAM), developed by Alexander Kirillov et al. in 2023, is a foundational model designed for general image segmentation tasks (Kirillov, A. et al., 2023). It employs an encoder-decoder architecture similar to that of U-Net, consisting of three primary components: an image encoder, a prompt encoder, and a mask decoder. The overall structure of SAM is depicted in Figure 3.

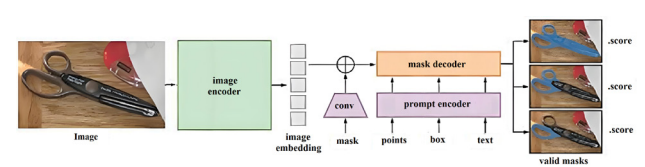


Figure. 3. Structure of the SAM model.

The image encoder in SAM is responsible for dimensionality reduction and feature extraction from the input image. The original image undergoes downsampling and is subsequently processed through convolutional layers to generate multiple sets of feature vectors. These features are further refined by multiple Transformer encoder layers to produce an image embedding, which is then passed to the decoder. The prompt encoder encodes various forms of prompts, including points, bounding boxes, text, and masks. The first three are categorized as sparse prompts, while masks are considered dense prompts. Different encoding strategies are employed for these prompt types, resulting in a prompt embedding that captures spatial location, category, and shape information. The mask decoder converts the combined image features and prompt embeddings into the final segmentation mask, comprising multiple upsampling and convolutional layers. Specifically, the decoder fuses features from the image encoder and prompt encoder, ensuring that both image content and input prompts influence the segmentation. The upsampling layers gradually restore the resolution of the feature maps to match the original image size, followed by convolutional operations that produce a probability mask aligned with the original image dimensions.

SAM is designed to segment objects of interest based on various prompts, such as single points, multiple points or masks, bounding boxes, and textual descriptions. The model is capable of generating valid segmentation masks even when prompts are ambiguous, requiring an understanding of the concept of "object" to perform accurate segmentation. This enables SAM to segment objects not present in the training data, demonstrating strong zero-shot generalization capabilities. The authors trained SAM on approximately 11 million images with 1.1 billion mask annotations, which contributed to its robust generalization performance in automatically segmenting objects without prompts. However, the masks produced by SAM lack semantic labels; thus, manual annotation or subsequent semantic segmentation is necessary to assign meaningful class labels to the segmented objects.

## **2.1.2** The U-Net

The U-Net model, introduced by Olaf Ronneberger et al. in 2015 (Ronneberger, O. et al., 2015), is a fully convolutional neural network characterized by a distinctive U-shaped architecture based on the Fully Convolutional Network (FCN). Originally designed for biomedical image segmentation, it has since become a fundamental architecture widely adopted in various image segmentation tasks due to its superior performance and robustness. The architecture of U-Net is depicted in Figure 4 and features a symmetric structure comprising an encoder, a decoder, and skip connections. The encoder, positioned on the left, functions as a backbone feature extractor, progressively reducing the spatial dimensions of the input while increasing the number of feature channels. Conversely, the decoder on the right aims to recover spatial resolution through successive upsampling, enabling precise localization. The skip connections directly concatenate feature maps from encoder layers to their corresponding decoder layers, facilitating the fusion of high-resolution spatial information with high-level semantic features, thereby reducing information loss and improving localization accuracy.

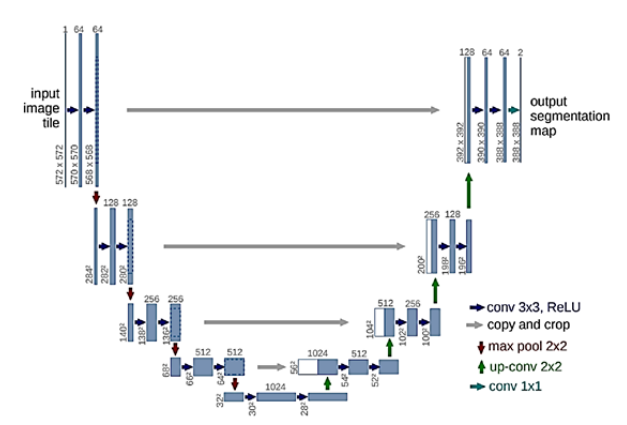


Figure. 4. Structure of the U-Net.

The encoder employs a repeated pattern of two convolutional layers, each with a 3×3 kernel, zero-padding, and ReLU activation functions, followed by a 2×2 max pooling operation with a stride of 2 for downsampling. Each downsampling step doubles the number of feature channels, with four such steps reducing the feature map size to 1/16 of the original spatial dimensions. The decoder reconstructs the feature maps through upsampling, utilizing 2×2 transposed convolution (or nearestneighbor upsampling) combined with convolutional layers of 3×3 kernels. Each upsampling step is followed by the concatenation with corresponding encoder feature maps, preserving spatial details. The convolutional layers in the decoder serve dual purposes: reducing feature man dimensionality and extracting salient features, with each pair of 3×3 convolutions followed by an activation. Upsampling halves the number of feature channels at each stage, and a final 1×1 convolutional layer restores the number of channels to produce the final semantic segmentation map. U-Net achieves highquality segmentation results even with limited training data, making it particularly suitable for applications where annotated datasets are scarce.

## 2.1.3 SAM assisted U-Net optimization

The optimization of the U-Net model, facilitated by the Segment Anything Model (SAM), is an iterative process designed to address the inefficiency associated with generating infrared images of power facility samples. As illustrated in Figure 5, this process comprises three primary steps: (1) generating annotation samples using SAM; (2) iteratively training the U-Net model with the generated samples; and (3) manually refining and correcting the samples until the dataset satisfies predefined quality and accuracy criteria.

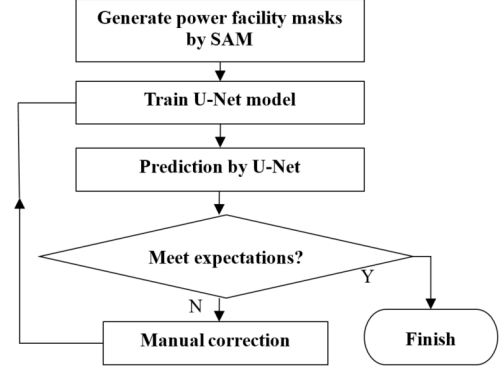


Figure. 5. Workflow of SAM assisted U-Net model optimization

The iterative optimization of the U-Net model, assisted by the Segment Anything Model (SAM), facilitates rapid construction of an infrared image dataset of power facilities. Due to the presence of unmasked regions that cannot be directly annotated,

this process essentially reduces to a binary semantic segmentation task—differentiating power facilities from all other regions in the image, including background and other categories. In this study, the U-Net architecture is employed, with the training procedure designed to exclude pixels belonging to non-power facility regions from the loss function calculation. The detailed workflow is as follows:

- 1. Utilize SAM to segment targets within the images and generate corresponding masks.
- 2. Based on the object masks produced by SAM, manually annotate all masks within a small subset of images, as illustrated in Figure 6. Each mask is assigned a uniform semantic label to all its pixels.
- 3. Train the U-Net model using these annotated images.
- 4. Apply the trained U-Net to predict semantic labels for masks in the remaining unannotated images. The predicted masks are then manually inspected, and any mislabeling is corrected. Corrected images are added to the training set for subsequent retraining.

By iterating steps 3 and 4, a large dataset of images with accurate masks and semantic labels can be efficiently generated.

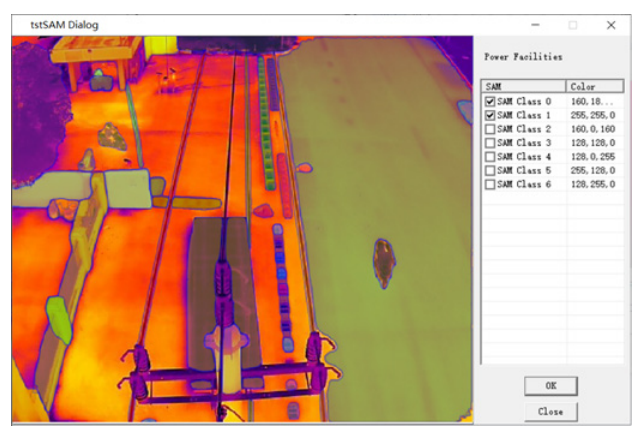


Figure. 6 Manually assigning SAM mask classification labels

#### 2.2 Dynamic temperature threshold model

The implicit fault detection method proposed in this study primarily relies on a temperature model. After estimating the temperature of power line components from infrared images, empirical thresholds are employed to identify potential hidden faults. However, these fixed thresholds are subject to variability under different environmental conditions, such as fluctuations in ambient temperature and solar irradiance, which introduce uncertainty and reduce the reliability of threshold-based fault detection. To address this issue, a comprehensive temperature model for electrical equipment is developed, incorporating factors such as ambient temperature, solar radiation, and self-heating effects. The model is expressed as follows:

$$T_r = a_0 T_E + a_1 T_P + a_2 T_S (1)$$

Where  $T_E$  denotes the ambient temperature, which can be directly obtained from meteorological station forecasts;  $T_P$  represents the self-heating of the electrical equipment, estimated based on the statistical power consumption of the line and typically considered a constant; and  $T_S$  indicates the temperature induced by solar radiation, determined by referencing solar radiation data from national environmental and meteorological websites according to the time and location of infrared data acquisition. In the model,  $a_0$ ,  $a_1$  and  $a_{20}$  are influence coefficients corresponding to ambient temperature, solar radiation, and self-heating effects, respectively, and are

initially unknown.

The main reason why we use a linear model here is that the model is very stable when there are not many data samples. We also tried a nonlinear model and found that it is very prone to overfitting, and its results are actually unreliable.

To determine the values of  $a_0$ ,  $a_1$  and  $a_{20}$  measured temperature data from all electrical facilities are substituted into the model, and linear regression is employed to estimate these coefficients. Once an accurate estimate of the equipment temperature is obtained, an empirical threshold method is applied for implicit fault detection. The thresholding approach primarily references the algorithm proposed by Wang et al. (2020) (Wang, B. et al., 2020), which compares the maximum temperature of the electrical component with the normal temperature  $T_{\text{norm}}$ .

If the temperature difference exceeds 1 K, further diagnostic rules, as detailed in Table 1, are applied. In these rules,  $T_{\rm norm}$  represents the baseline temperature under normal conditions;  $T_{ab}$  denotes the average temperature of the abnormal region;  $T_{th}$  is the warning temperature threshold, set as 1.2 times  $T_{\rm norm}$  ased on historical data; and  $\alpha$  indicates the proportion of pixels within the abnormal region.

Discriminant criteria	Temperature conditions	Fault
$T_{norm} < T_{ab} < T_{th}$ $A > 70\%$	The overall temperature rise of the insulator is relatively small	The resistance of the insulator is very small
$T_{norm} < T_{ab} < T_{th}$ $A < 30\%$	There is a slight temperature rise in the insulator section	Insulators indicate the presence of partial discharge or contamination
T <sub>ab</sub> > T <sub>th</sub> A<30%	There is a significant temperature rise and a small temperature rise in the insulator part	Insulators are damaged and may have cracks
T <sub>ab</sub> > T <sub>th</sub> A>70%	The overall temperature rise of the insulator is relatively large	The insulator has a serious malfunction

**Table 1**. The fault recognition experience threshold (Wang, B., et al., 2020)

## 3. Experimental

## 3.1 Experimental dataset and environment

In the experimental section of this study, a DJI M3T unmanned aerial vehicle(UAV) served as the flight platform, quipped with a thermal infrared camera for capturing infrared imagery of power lines. The UAV and its onboard camera are illustrated in Figure 7, and the camera specifications are summarized in Table 2.



Figure. 7. Image of equipment (a) DJI-M3T drone and (b) M3T dual-camera

	Infrared	Visible
Image	640×512pixels	8000×6000pixels
Resolution	1280×1024 pixels	
Pixels Size	12 μm	3.67µm
Focus Length	40 mm	24 mm
Image Format	R-JPEG (16 bit)	JPEG(8 bit)
DFOV	40.6°	84°
GPS Info	Yes	Yes
Gimbal Info	Yes	Yes

Table 2 Technical specifications of M3T dual-camera

The M3T dual-camera system simultaneously captures visible light and infrared images. In this experiment, a total of 3094 infrared images were obtained over 9 sorties, with some sample images shown in Figure 8.

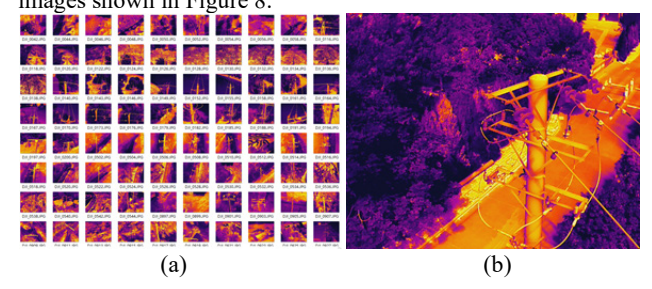


Figure. 8. The infrared images (a)The thumbs of infrared images (b)A infrared image

The experiments were conducted on Windows 10 using an NVIDIA GeForce RTX 3060 12G GPU. The deep learning framework was built on PyTorch 1.12 and CUDA 11.6. The UNET COMES from Milesial's source code provided on GitHub. The download link is:

https://github.com/milesial/Pytorch-UNet/tree/v1.0

## 3.2 SAM classification

A total of 750 images were randomly selected from the original dataset comprising 3,094 images and manually annotated using the SAM-assisted annotation method proposed in this study (the annotation interface is shown in Fig. 6. The objective was to accurately label power facilities—including transmission towers, power lines, insulators, and various connecting wires—to generate corresponding mask files. The annotation results are illustrated in Fig. 9.

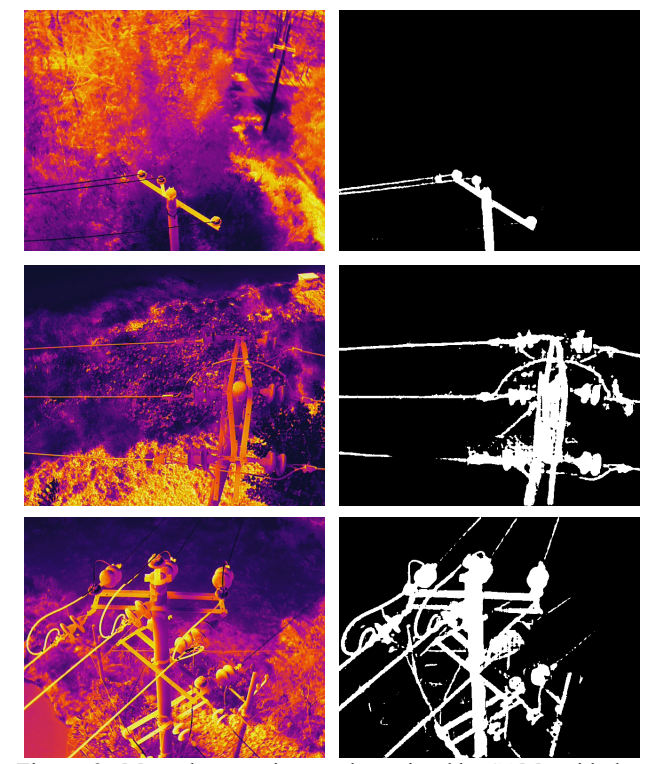


Figure. 9. Manual annotation results assisted by SAM, with the infrared image on the left and the power facility mask on the right

Due to the slender structure of power lines occupying minimal pixels in infrared imagery, their classification performance was relatively poor. In contrast, transmission towers and insulators demonstrated significantly better classification results, owing to their more prominent appearance in infrared images. Additionally, some images contained power facilities that were barely visible (as shown in Fig. 10). These images were subsequently excluded from the dataset, resulting in a final set of 725 valid images for further analysis.

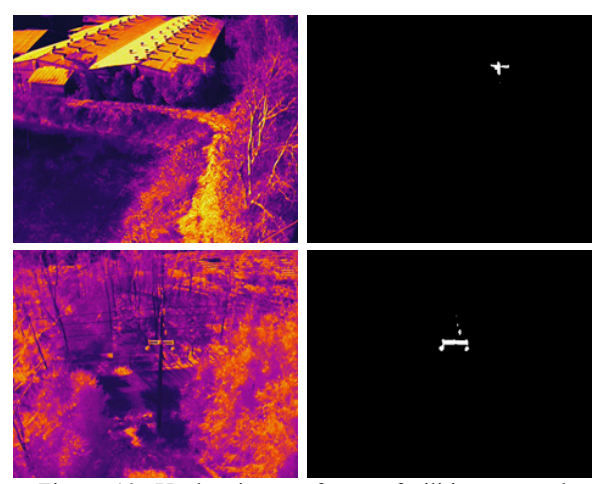


Figure. 10. Unclear image of power facilities removed

#### 3.3 U-Net train

The 725 samples were trained using the U-Net architecture with hyperparameters listed in Table 3.

Hyperparameter	Value	
Epochs	5	
BatchSize	8	
Learning rate	0.01	
Training size	580 (80%)	
Test size	145 (20%)	

Table 3 The hyperparameters for first training

After the initial training phase, the training loss curve is presented in Figure. 11.

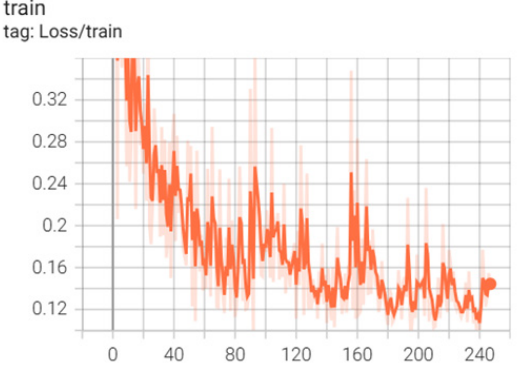


Figure. 11. The loss rate curve of the first training

The learning rate progression during training is visualized in Figure. 12.

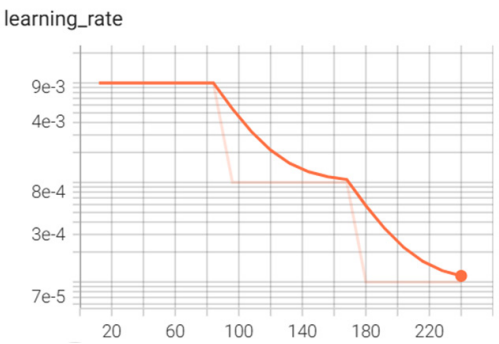


Figure. 12. The learning rate curve for first training

Validation accuracy on the test set is shown in Figure. 13

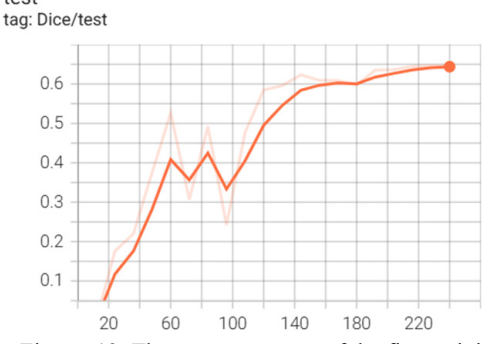


Figure. 13. The accuracy curve of the first training

Representative segmentation results from the test set are displayed in Figure. 14.

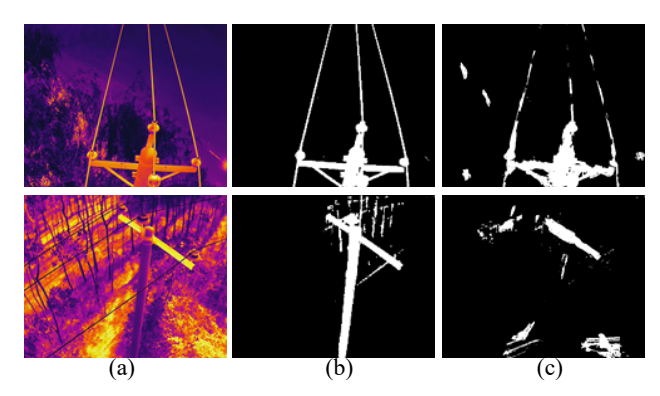


Fig. 14. Test image processing results after initial training (a) Input image (b) True value (c) Predicted value

Despite suboptimal performance on the test set, we employed the trained model to predict unlabeled images. Well-performing predictions were manually selected and incorporated into the training dataset through an iterative process repeated 10 times. This data augmentation strategy ultimately expanded the training dataset to 2773 samples, which was subsequently used for retraining. The loss curve from the final training iteration is presented in Figure. 15.

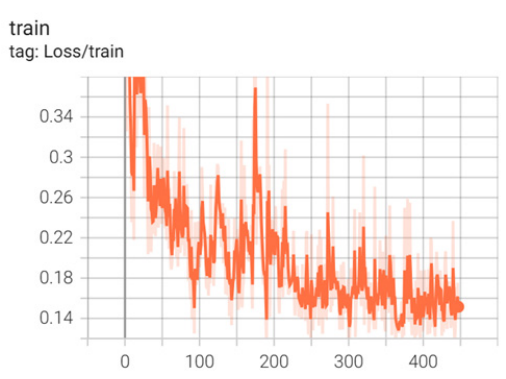


Figure. 15. The loss rate curve of the final training

The learning rate curve for the final training iteration is presented in Figure. 16

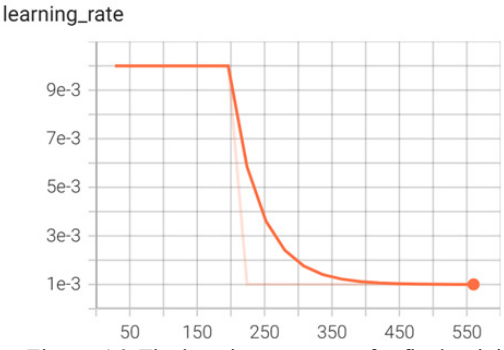


Figure. 16. The learning rate curve for final training

The corresponding test set accuracy curve is shown in Figure. 17.

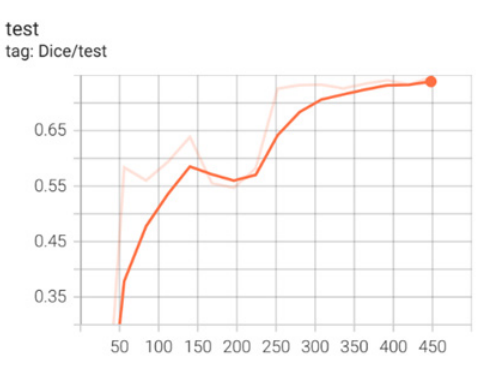


Figure. 17. The accuracy curve of the final training

Segmentation results obtained using the final trained model are visualized in Figure. 18.

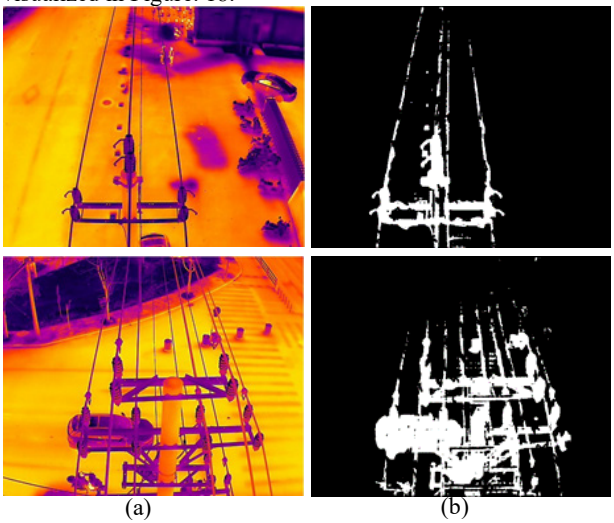


Fig. 18. Prediction result after the last training (a) Input image (b) Prediction value

While the results exhibited certain limitations, including incomplete power line detection and over-segmentation of transmission towers, the identification accuracy for insulators remained satisfactory. Given that most power line connections are located near insulators, we concluded that these results provide sufficient foundation for subsequent latent fault analysis.

## 3.4 Hidden fault detection

The total 2773 images identified by SAM and predicted by U-Net, along with their corresponding mask data, were input into Equation (2-1) with parameters set as TE=19 °C, TP=10 °C, and TS=12 °C. The equipment temperature was calculated as the mean value of the entire mask temperature distribution. Through least squares fitting, the coefficients were determined as a0=1.04, a1=0.06, and a2=0.13. Subsequently, the fitted results from Equation (2-1) were considered as the ideal temperature reference.

Subsequently, anomaly detection was conducted on the hottest regions within the 2,773 images and their masks, based on the threshold criteria defined in Table 1. To mitigate the influence of noise-induced temperature fluctuations, median filtering with a 25×25 kernel was applied to the temperature data of all images. This process identified four anomalies, as illustrated in Figures 19, 20, 21, and 22.

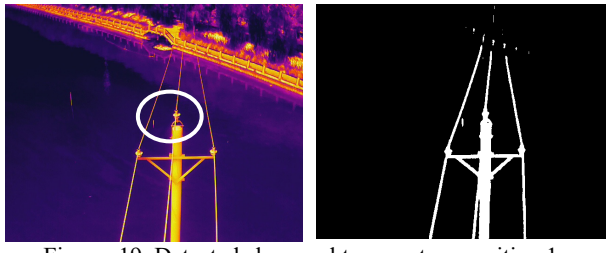


Figure. 19. Detected abnormal temperature position 1

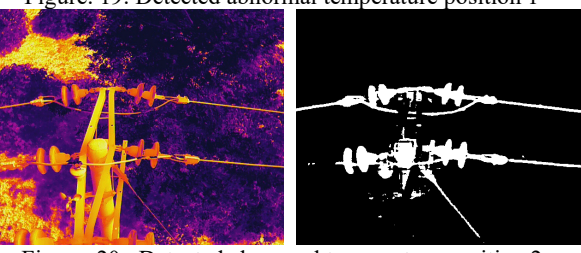


Figure. 20. Detected abnormal temperature position 2

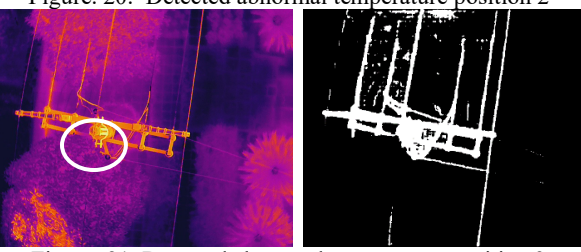


Figure. 21. Detected abnormal temperature position 3





Figure. 22. Detected abnormal temperature position 4

Among the analyzed images, three contained actual anomalies (Figures 20, 21, and 22). The anomaly detected in Figure 19 was determined to be a false positive. Based on these results, the proposed method achieved a preliminary detection recall of 100% and a precision rate of 75%.

### 3.5 Limitations

The current study has the following limitations:

- (1)This research focuses more on addressing specific engineering problems and does not propose significant theoretical advancements in algorithmic innovation.
- (2)The parameters used for abnormal temperature detection are only validated in this specific case. Due to the lack of open-source datasets, their effectiveness has not been verified on other data.

## 4. Conclusion

This study presents a methodology for detecting hidden faults in power infrastructure using thermal infrared imagery. The approach integrates three key components:

- (1) rapid annotation facilitated by the SAM model to efficiently label power components in infrared images;
- (2) iterative refinement of a U-Net architecture using annotated data to enable automated component recognition; and
- (3) anomaly detection through a combination of temperature analysis and threshold segmentation to identify latent faults.

Field validation was performed on a transmission line in Jiaxing City, Zhejiang Province, where a DJI M3T UAV captured 3,094 thermal images. Of these, 725 images were manually annotated with SAM, and subsequent data augmentation with the U-Net model resulted in 2,773 images with integrated masks. Threshold-based segmentation identified four anomalies, three of which corresponded to confirmed faults within the test area. Although one false positive was observed, the overall detection performance achieved a recall of 100% and a precision of 75%. These results demonstrate the effectiveness of the proposed method for hidden fault detection in power infrastructure, providing a promising tool for maintenance and safety assurance.

#### References

- Impram, S., Nese, S. V., & Oral, B. (2020). Challenges of renewable energy penetration on power system flexibility: A survey. \*Energy Strategy Reviews, 31\*, 100539. https://doi.org/10.1016/j.esr.2020.100539
- Strielkowski, W., Civín, L., Tarkhanova, E., Tvaronavičienė, M., & Petrenko, Y. (2021). Renewable energy in the sustainable development of electrical power sector: A review. \*Energies, 14\*(24), 8240. https://doi.org/10.3390/en14248240
- Dashti, R., Daisy, M., Mirshekali, H., Shaker, H. R., & Hosseini Aliabadi, M. (2021). A survey of fault prediction and location methods in electrical energy distribution networks. \*Measurement, 184\*, 109947. https://doi.org/10.1016/j.measurement.2021.109947
- Abro, G. E. M., Ali, A., Memon, S. A., Memon, T. D., & Khan, F. (2024). Strategies and challenges for unmanned aerial vehicle-based continuous inspection and predictive maintenance of solar modules. \*IEEE Access, 12\*, 176615–176629. https://doi.org/10.1109/ACCESS.2024.3505754
- Barbedo, J. G. A. (2019). A review on the use of unmanned aerial vehicles and imaging sensors for monitoring and assessing plant stresses. \*Drones, 3\*(2), 40. https://doi.org/10.3390/drones3020040
- Susakova, T. V., Evseeva, A. M., & Chesnokova, I. A. (2017). Analysis and prevention of accident-caused faults in power cable lines. \*MATEC Web of Conferences, 110\*, 01077. https://doi.org/10.1051/matecconf/201711001077
- Liao, W., Yang, D., Wang, Y., & Ren, X. (2021). Fault diagnosis of power transformers using graph convolutional network. \*CSEE Journal of Power and Energy Systems, 7\*(2), 241–249. https://doi.org/10.17775/CSEEJPES.2020.04120
- Mateus, B. C., Farinha, J. T., & Mendes, M. (2024). Fault detection and prediction for power transformers using fuzzy logic and neural networks. \*Energies, 17\*(2), 296. https://doi.org/10.3390/en17020296
- McManus, C., Tanure, C. B., Peripolli, V., Seixas, L., Fischer, V., Gabbi, A. M., Menegassi, S. R. O., Stumpf, M. T., Kolling, G. J., Dias, E., & Costa, J. B. G. (2016). Infrared thermography in animal production: An overview. \*Computers and Electronics in Agriculture, 123\*, 10–16. https://doi.org/10.1016/j.compag.2016.01.027
- Hou, F., Zhang, Y., Zhou, Y., Zhang, M., Lv, B., & Wu, J. (2022). Review on infrared imaging technology.

- \*Sustainability, 14\*(18), 11161. https://doi.org/10.3390/su141811161
- Cheng, F., Niu, B., Xu, N., Zhao, X., & Ahmad, A. (2023). Fault detection and performance recovery design with deferred actuator replacement via a low-computation method. \*IEEE Transactions on Automation Science and Engineering, 20\*(4), 1–11. https://doi.org/10.1109/TASE.2023.3300723
- Hedayati, M., Barzegar, A., & Rahimi, A. (2024). Fault diagnosis and prognosis of satellites and unmanned aerial vehicles: A review. \*Applied Sciences, 14\*(20), 9487. https://doi.org/10.3390/app14209487
- Sarabandi, K., & Park, M. (2002). Extraction of power line maps from millimeter-wave polarimetric SAR images. \*IEEE Transactions on Antennas and Propagation, 48\*(12), 1802–1809. https://doi.org/10.1109/TAP.2002.805248
- Mira, J. L., Barba, J., Romero, F. P., et al. (2024). Benchmarking of computer vision methods for energy-efficient high-accuracy olive fly detection on edge devices. \*Multimedia Tools and Applications, 83\*, 81785–81809. https://doi.org/10.1007/s11042-024-18589-y
- Wang, G., Zhang, L., Sun, H., & Zhu, C. (2021). Longitudinal tear detection of conveyor belt under uneven light based on Haar-AdaBoost and Cascade algorithm. \*Measurement, 168\*, 108341. https://doi.org/10.1016/j.measurement.2020.108341
- Zhang, J., Liu, L., Wang, B., Chen, X., Wang, Q., & Zheng, T. (2012). High speed automatic power line detection and tracking for a UAV-based inspection. \*2012 International Conference on Industrial Control and Electronics Engineering\* (pp. 266–269). Xi'an, China. https://doi.org/10.1109/ICICEE.2012.77
- Seikh, N., & Mollah, A. F. (2022). Power line detection from aerial vehicles using Hough transform. \*2022 IEEE Calcutta Conference (CALCON)\* (pp. 1–3). Kolkata, India. https://doi.org/10.1109/CALCON56258.2022.10060117
- Ma, W., et al. (2024). Transmission tower and power line detection based on improved Solov2. \*IEEE Transactions on Instrumentation and Measurement, 73\*, 5015711. https://doi.org/10.1109/TIM.2024.3381713
- Zheng, X., Pan, B., & Zhang, J. (2020). Power tower detection in remote sensing imagery based on deformable network and transfer learning [In Chinese]. \*Acta Geodaetica et Cartographica Sinica, 49\*(8), 1042–1050. https://doi.org/10.11947/j.AGCS.2020.20190356
- Zhao, Q., Fang, H., Pang, Y., et al. (2025). PL-UNet: A real-time power line segmentation model for aerial images based on adaptive fusion and cross-stage multi-scale analysis. \*Journal of Real-Time Image Processing, 22\*, 39. https://doi.org/10.1007/s11554-024-01615-5
- Nan, G., Li, H., Du, H., Liu, Z., Wang, M., & Xu, S. (2024). A semantic segmentation method based on AS-Unet++ for power remote sensing of images. \*Sensors, 24\*(1), 269. https://doi.org/10.3390/s24010269
- He, M., Qin, L., Deng, X., Zhou, S., Liu, H., & Liu, K. (2023). Transmission line segmentation solutions for UAV aerial photography based on improved UNet. \*Drones, 7\*(4), 274. https://doi.org/10.3390/drones7040274

- Zou, X. (2019). A review of object detection techniques. \*2019 International Conference on Smart Grid and Electrical Automation (ICSGEA)\* (pp. 251–254). Xiangtan, China. https://doi.org/10.1109/ICSGEA.2019.00065
- Kaur, R., & Singh, S. (2023). A comprehensive review of object detection with deep learning. \*Digital Signal Processing, 132\*, 103812. https://doi.org/10.1016/j.dsp.2022.103812
- Manakitsa, N., Maraslidis, G. S., Moysis, L., & Fragulis, G. F. (2024). A review of machine learning and deep learning for object detection, semantic segmentation, and human action recognition in machine and robotic vision. \*Technologies, 12\*(2), 15. https://doi.org/10.3390/technologies12020015
- Islam, M. I., Jadin, M. S., Mansur, A. A., & Alharbi, T. (2024). Electrical performance and degradation analysis of field-aged PV modules in tropical climates: A comparative experimental study. \*Energy Conversion and Management: X, 24\*, 100719. https://doi.org/10.1016/j.ecmx.2024.100719
- Junior, O. S., Coninck, J. C. P., Magrin, F. G. S., Ganacim, F. I. S., Pombeiro, A., Fernandes, L. G., & Romaneli, E. F. R. (2023). Impacts of atmospheric and load conditions on the power substation equipment temperature model. \*Energies, 16\*(11), 4295. https://doi.org/10.3390/en16114295
- Zhu, M., Ma, D., Zhou, Y., Huang, H., Shao, Z., Wu, F., & Li, B. (2024). The change of sealing property in the aging process of NBR sealing equipment based on finite element analysis. \*Coatings, 14\*(9), 1178. https://doi.org/10.3390/coatings14091178
- Wan, Q., Brede, B., Smigaj, M., & Kooistra, L. (2021). Factors influencing temperature measurements from miniaturized thermal infrared (TIR) cameras: A laboratory-based approach. \*Sensors, 21\*(24), 8466. https://doi.org/10.3390/s21248466
- Felbermayr, G., Gröschl, J., Sanders, M., Schippers, V., & Steinwachs, T. (2022). The economic impact of weather anomalies. \*World Development, 151\*, 105745. https://doi.org/10.1016/j.worlddev.2021.105745
- Luo, C., Huang, L., Gong, Y., & Ma, W. (2012). Thermodynamic comparison of different types of geothermal power plant systems and case studies in China. \*Renewable Energy, 48\*, 155–160. https://doi.org/10.1016/j.renene.2012.04.037
- Kirillov, A., et al. (2023). Segment anything. \*2023 IEEE/CVF International Conference on Computer Vision (ICCV)\* (pp. 3992–4003). Paris, France. https://doi.org/10.1109/ICCV51070.2023.00371
- Ronneberger, O., Fischer, P., & Brox, T. (2015). U-Net: Convolutional networks for biomedical image segmentation. In N. Navab, J. Hornegger, W. Wells, & A. Frangi (Eds.), \*Medical Image Computing and Computer-Assisted Intervention MICCAI 2015\* (pp. 234–241). Springer. https://doi.org/10.1007/978-3-319-24574-4 28
- Wang, B., et al. (2020). Automatic fault diagnosis of infrared insulator images based on image instance segmentation and temperature analysis. \*IEEE Transactions on Instrumentation and Measurement, 69\*(8), 5345–5355. https://doi.org/10.1109/TIM.2020.2965635